Vacancies-engineered MoO₃ and Na⁺-preinserted MnO₂ *in-situ* grown N-doped graphene nanotubes as electrode materials for high-performance asymmetric supercapacitor

Jian Zhao[a], He Cheng[a], Huanyu Li[a], Yan-Jie Wang[b]*, Qingyan Jiang[d], Lina Yang[a], Alan Meng[a], Jianfeng Huang[e], Changlong Sun[a], Huifang Li[a], Zhenjiang Li[a]* and Jiujun Zhang[c]*

[a]*College of Materials Science & Engineering, College of Electromechanical Engineering, College of Chemistry and Molecular Engineering, Qingdao University of Science and Technology, Qingdao 266042, Shandong, P. R. China.*

[b]*New Energy and Advanced Functional Materials Group, School of Materials Science and Engineering, Dongguan University of Technology, Dongguan 523808, Guangdong, P. R. China*

[c]*Institute for Sustainable Energy/College of Sciences, Shanghai University, 99 Shangda Rd, Baoshan, Shanghai 200444, P.R. China*

[d]*Ocean College, Zhejiang University, Zhoushan 316021, Zhejiang, P. R. China.*

[e]*School of Material Science and Engineering, Shaanxi University of Science and Technology, Xi'an 710021, Shaanxi, P. R. China.*

***Corresponding Author**

E-mail: jiujun@shaw.ca (J. Zhang);
       zjli126@126.com (Z. Li);
       wyj@dgut.edu.cn (Y. Wang)

Calculations:

(1) The specific capacitances of the prepared electrodes calculated from GCD curves are obtained according to the following equation:

$$C = \frac{I\Delta t}{m\Delta V}$$

$$(S\text{-}1)$$

where I is the discharge current, Δt is the discharge time in GCD test, m is the active material mass, and ΔV is the voltage window.

(2) The specific capacitance of the obtained asymmetric supercapacitor (ASC) device can be obtained in accordance with the following equation:

$$C_{device} = \frac{I\Delta t}{M\Delta V}$$

$$(S\text{-}2)$$

Herein, I is the discharge current, Δt is the discharge time in GCD test, M is the total mass of both the positive and negative electrodes, and ΔV is the voltage window of the device.

(3) Methods to calculate the energy and power density of the ASC device:

$$E = \frac{1}{2}C_{device}\Delta V^2 ; \ P = \frac{E}{t} \quad (S\text{-}3)$$

Here, C_{device} is the specific capacitance of the device, ΔV is the potential window, and t is the discharge time.

Experimental section:

Chemicals and Materials: **Ammonium molybdate ($(NH_4)_6Mo_7O_{24}\cdot4H_2O$), sodium sulfate ($Na_2SO_4$) and potassium permanganate ($KMnO_4$) were purchased from Sinopharm Chemical Reagent Co., Ltd. All the chemical reagents were AR grade and used without further purification. In addition, fiber separator and commercial graphite substrates were procured from Sinopharm Chemical Reagent Co., Ltd and Qingdao kanglong graphite Co. Ltd, respectively.**

Fabrication of N-GNTs deposited on the graphite wafer: The N-GNTs were fabricated via chemical vapor reactions (CVR) in a traditional high-temperature vacuum furnace. The detailed experimental procedure can be referred to our previous reports.[1,2]

Preparation of N-GNTs@MoO$_{3-x}$ nanochains on the graphite wafer: The N-GNTs@MoO$_{3-x}$ nanochains were synthesized by electrodeposition, calcination and reduction treatment processes. Firstly, an electrodeposition was performed in a standard three-electrode configuration, where the N-GNTs, a Pt wire and a saturated calomel (SCE) were used as the working electrode, counter electrode and reference electrode, respectively. The amorphous Mo-O was electrodeposited on N-GNTs skeleton in a 10 mmolL^{-1} $(NH_4)_6Mo_7O_{24}\cdot4H_2O$ aqueous electrolyte utilizing a CHI660E Electrochemical Workstation at -10 mA cm^{-2} for 200 seconds. Secondly, the obtained N-GNTs@ amorphous Mo-O was transformed into N-GNTs@MoO$_3$ through a calcination at 350 °C for 1 hour at a ramping rate of 2 °C min^{-1} in air atmosphere. Finally, N-GNTs@MoO$_{3-x}$ nanochains were obtained by immersing the

above products in 0.1 M KBH$_4$ solution for 3 minutes. For comparison, the N-GNTs@MoO$_3$, N-GNTs@Mo-O, bare MoO$_3$ and Mo-O were also fabricated on graphite wafers by the above technique with the same experimental conditions. The mass loading of active materials for N-GNTs@Mo-O, N-GNTs@MoO$_3$ and N-GNTs@MoO$_{3-x}$ were about 1.0, 1.3 and 1.1 mg cm^{-2}, respectively.

Computational details: The calculations were conducted utilizing the periodic density-functional theory (DFT) framework implemented in the CASTEP module of Materials Studio 6.1 using the Perdew-Burke-Emzerhof (PBE) functional and ultrasoft pseudopotential (USPP) method.[3-6] For bulk MoO$_3$, a cut-off kinetic energy of 500 eV, a 1×3×2 Monkhorst-pack k-point (Γ point) mesh, and a smearing of 0.1 eV were applied during the geometric optimization. The convergence criteria of the self-consistent field (SCF), total energy difference, maximum force, and maximum displacement were $2.0×10^{-6}$ eV/atom, $2.0×10^{-5}$ eV/atom, $5.0×10^{-2}$ eV/Å, and $2.0×10^{-3}$ Å, respectively. Based on the optimized MoO$_3$, a 4 × 2 × 1 supercell with vacuum thickness of 12 Å was built to model the MoO$_3$ (010) facet. The plane-wave cutoff was tested by varying the parameter between 300 and 600 eV. Convergence was achieved with a cutoff energy of 500 eV. For the sake of simplicity, graphene tube is replaced by graphene nanosheet in all calculations. Based on the CASTEP-optimized surfaces, the adsorption of Na$^+$ on the pristine surface or surfaces with oxygen vacancy was modeled, and the adsorption energy was calculated by:

$$E_{ads}= E_{MoO3(Na^+)}- E_{MoO3} -2E_{Na^+} \quad \text{or} \quad E_{ads}= E_{MoO3-x(Na^+)}- E_{MoO3-x} -2E_{Na^+}$$

(3)

where $E_{MoO3(Na^+)}$ or $E_{MoO3-x(Na^+)}$ is the energy of the Na$^+$ adsorbed surface, E_{MoO3} or E_{MoO3-x} is the energy of the stable surface, and E_{Na^+} is the energy of Na$^+$.

Preparation of N-GNTs@Na$_x$MnO$_2$ nanosheet arrays on the graphite wafer: The N-GNTs@Na$_x$MnO$_2$ nanosheet arrays were synthesized by the water bath heating and an electrochemical method. Firstly, 0.01 mol L^{-1} KMnO$_4$ was dissolved into 50 mL of distilled water. The obtained solution was transferred into a beaker, and then a piece of graphite wafer (1 x 1 cm^{-2}) with N-GNTs was also immersed into the solution. Secondly, the beaker was heated at 90 °C for 20 minutes in water bath. After cooling down to the room temperature naturally, the precursors MnO$_2$ grown on N-GNTs was taken out. Finally, the N-GNTs@Na$_x$MnO$_2$ nanosheet arrays were achieved by CV scans between 0 and 1.3 V in 5 m mol L^{-1} Na$_2$SO$_4$ electrolyte for 30 cycles with N-GNTs@MnO$_2$ as the working electrode, Pt wire and Ag/AgCl were used as the counter and reference electrodes. The mass loading of active materials for N-GNTs@Na$_x$MnO$_2$ was about 1.2 mg cm^{-2}.

Assembly of an asymmetric supercapacitor (ASC): An ASC device was assembled using N-GNTs@MoO$_{3-x}$ and N-GNTs@Na$_x$MnO$_2$ as the negative and positive electrodes, respectively, and the filter paper was employed as the separator. The typical mass loadings of the positive and negative electrode active materials were determined according to the well-known charge balance theory.[S7]

Materials Characterization: FESEM (Hitachi, SU8010) and TEM (Hitachi, H-8100) were employed to study the microstructural information of the obtained electrode materials. XRD (D8 X-ray diffractometer) was used to achieve the phase

compositions. XPS technique was carried out to further identify the surface composition on a Thermo ESCALAB 250Xi device with an Al-Kα (hν=1486.6 eV) excitation source. Meanwhile, for characterizing the oxygen vacancies features of the samples, electronic paramagnetic resonance (EPR, JES-FA200) was performed at X-band (~9.4 GHz) with a resolution of 2.44 μT. Mo K-edge extended X-ray absorption fine structure (EXAFS) spectroscopy were carried out at the beamline 1W1B of Bejing Synchrotron Radiation Facility. The electron beam energy of the storage ring was 2.5 GeV with ~250 mA.

Electrochemical measurements: Cyclic voltammetry (CV), Galvanostatic charge-discharge (GCD) and electrochemical impedance spectroscopy (EIS) were measured using an electrochemical instrument of CHI660e (Chenhua Instrument Co., Shanghai, China). The capacitive performances of the obtained electrodes were studied in a standard three-electrode systems with Pt wire and a Hg/HgO as the counter and reference electrode, respectively. Moreover, the electrochemical properties of the ACS were tested in a two-electrode configuration.
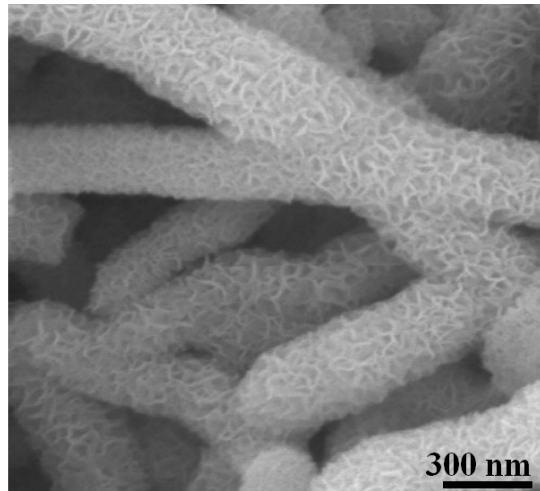
Fig. S1. SEM image of the MnO$_2$ nanosheet arrays.
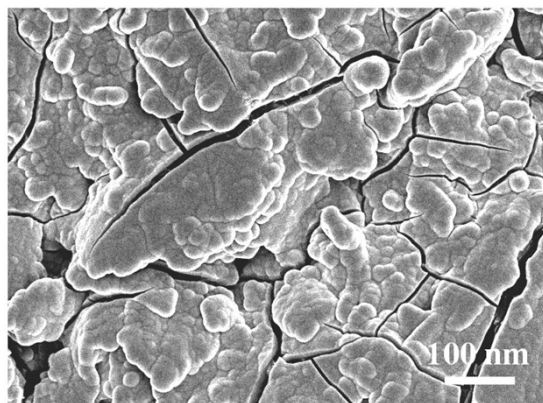
Fig. S2. SEM image of the bare MoO$_3$ directly grown on the graphite substrate.
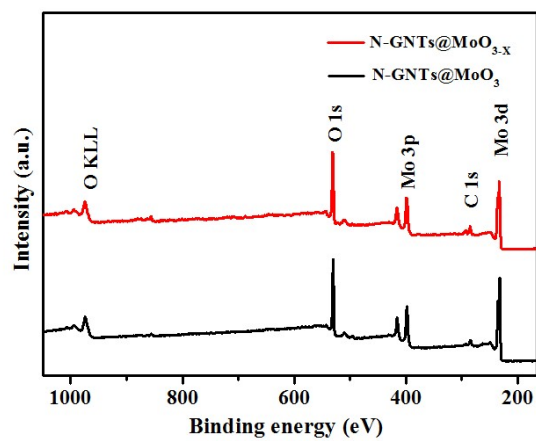
Fig. S3. XPS survey spectra of N-GNTs@MoO$_{3-x}$ and N-GNTs@MoO$_3$.
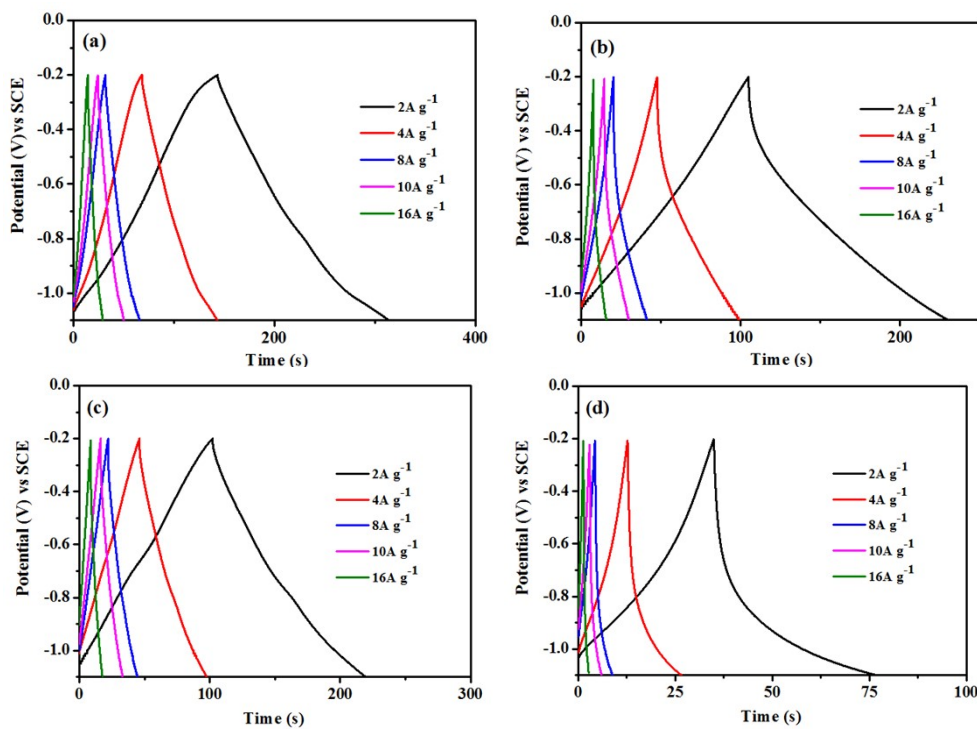
Fig. S4. GCD curves of N-GNTs@MoO3 (a), N-GNTs@Mo-O (b), MoO3 (c) and Mo-O (d).

Table S1. Comparison of the electrochemical properties of the as-fabricated N-GNT@MoO$_{3-x}$ with previously reported negative electrode materials.

Material	Fabrication method	Specific capacitance (F g^{-1})	Rate performance	Reference
MoO$_2$/GC-NTs	Self-Assembly Method	311.1(0.2 A g^{-1})	185.2(5A g^{-1})	8
FeOOH	electrodeposition	315 (0.5 A g^{-1})	194 (10 A g^{-1})	9
Bi$_2$S$_3$	Hydrothermal and calcination	466 (1 A g^{-1})	299 (8 A g^{-1})	10
GNC	Hummers and calcination	176（0.5 A g^{-1}）	142(10 A g^{-1})	11
RGO@VO$_2$	Hydrothermal	326 (0.85 A g^{-1})	188(17 A g^{-1})	12
FC@FeCo/NHCS	calcination	302 (0.2 A g^{-1})	185.5(10 A g^{-1})	13
Bi$_3$O$_2$	Hydrothermal	559 (0.4 A g^{-1})	11(1.8 A g^{-1})	14
N-OMCS	calcination	288(0.1 A g^{-1})	49(50 A g^{-1})	15
HPCS	calcination	576(1 A g^{-1})	267(20 A g^{-1})	16
2D/2D-SnS$_2$/MoS$_2$	hydrothermal method	466（1A g^{-1}）	209(8A g^{-1})	17
N-GNT@MoO$_{3-x}$	**Electrodeposition, calcination and reduction treatment**	**591 (2 A g^{-1})**	**445 (16 A g^{-1})**	**In this work**
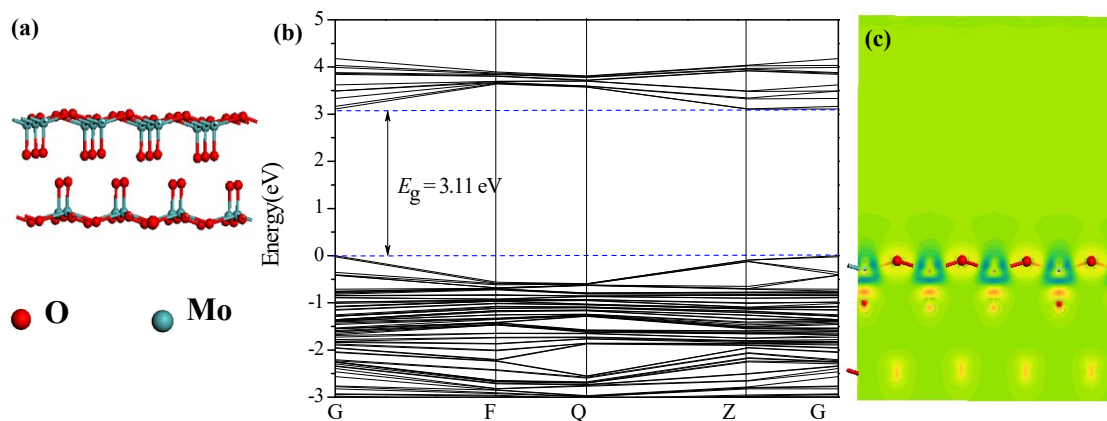
Fig. S5. Optimized structures (a), band structures (b) and charge density map (c) of the bare MoO_3.
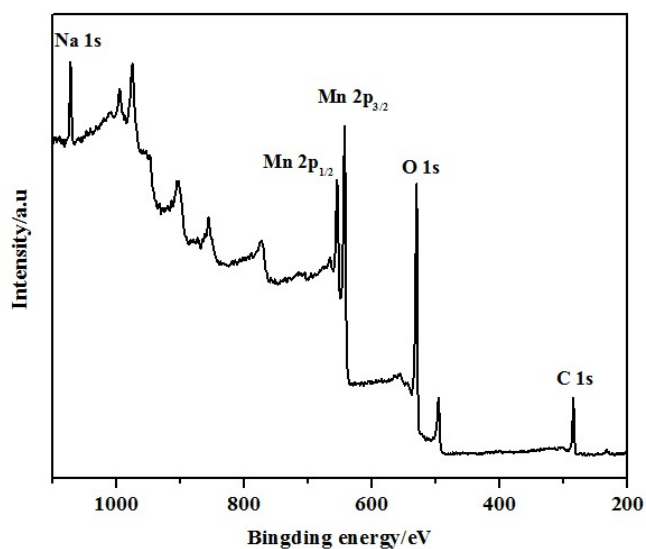
Fig. S6. XPS survey spectra of the N-GNTs@Na$_x$MnO$_2$.

Table S2. Electrochemical performances comparison of the as-prepared N-GNT @Na$_x$MnO$_2$ with other Mn-based compound positive electrodes fabricated by different methods.

Material	Fabrication method	Specific capacitance ($F\,g^{-1}$)	Potential window (V)/VS. SCE	Reference
graphene@Mn_3O_4	Calcination and water bath	208.3(0.5 A g^{-1})	0-0.81	18
Mn_3O_4/RGO	Air oxidation	166(0.1 A g^{-1})	0-0.9	19
Si-diatom@MnO_2	Calcination and Hydrothermal	341.5(0.5 A g^{-1})	-0.2-0.8	20
$La_{1-x}Sr_xMnO_3$	Solution reaction	102(1 A g^{-1})	0-0.5	21
ε-MnO_2/$Ti_3C_2T_x$	chemical synthesis	212.1(1 A g^{-1})	0-0.7	22
MnO2-AgCNT-CC	Electrodepositi-on	325(1 A g^{-1})	0-0.8	23
α-MnO_2 nanowires@ultrathin δ-MnO_2	Hydrothermal and chemical bath deposition	312(0.5 A g^{-1})	-0.1-0.55	24
ε-MnO_2 nanosheets //secondary α-MnO_2 nanorods.	Electrodepositi-on chemical bath	304(0.3 A g^{-1})	0-0.9	25
MnO_2/RGO	Hydrothermal	290(1 A g^{-1})	0-0.8	26
$Mn0_2$/GH	Calcination	200.6(1 A g^{-1})	0-1.0	27
N-GNT@Na_xMnO_2	**Hydrothermal and Electrodepositi-on**	**429(1.5A g^{-1})**	**1.2(SCE)**	**In this work**
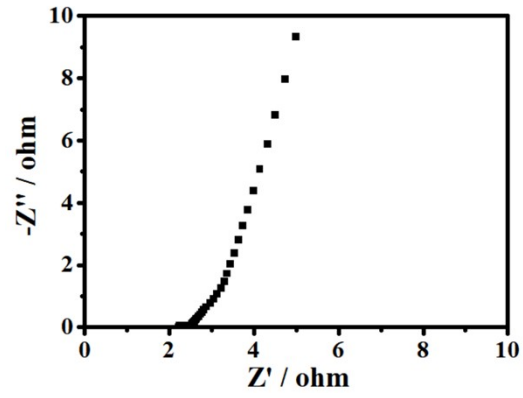
Fig. S7. The EIS pattern of N-GNTs@NaxMnO$_2$ positive electrode.
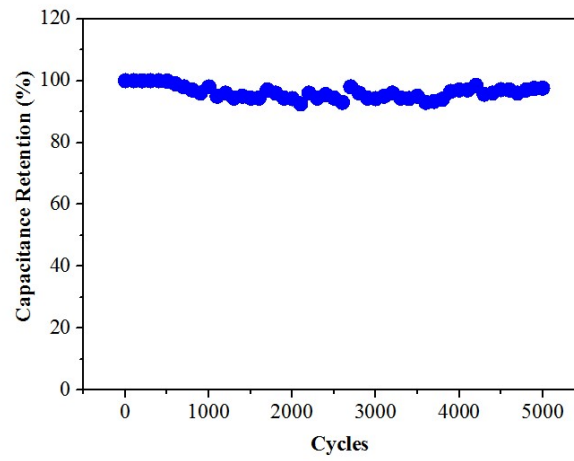
Fig. S8. Cycle property of the N-GNTs@Na$_x$MnO$_2$ after 5000 cycles.

Table S3. Cycle performance comparison of the assembled ASC with other state-of-the-art ASC devices with various positive and negative electrodes.

ASC devices	Cell voltage (V)	electrolyte	Cycle performance	Reference
Bi_2O_3//$MnCO_3QDs$/NiH−Mn−CO_3	1.5	6M KOH	81% retention after 5000 cycles	28
$Ni(OH)_2$-CoQD//RGO	1.45	2M KOH	84.1% retention after 5000 cycles	29
GrP/10-MnO2//GrP	1.6	0.05M Na_2SO_4	82.2%retention after 5000 cycles	30
ZNCN//FeOOH)	1.6	2 M KOH	77 %retention after 5000 cycles	31
$MoSe_2$/G//AC SICs	1.6	0.5MH_2SO_4	81% retention after 5000 cycles	32
NiS@CoS//AC	1.7	2 M KOH	80%retention after 5000 cycles	33
NCLDH@CNTs//AC	1.5	6M KOH	78.7%retention after 5000 cycles	34
B-Bi_2O_3//$MnCO_3QDs$/NiH–Mn–CO_3	1.5	6M KOH	81%retention after 5000 cycles	35
NiNTAS@Fe2O3//NiNTAS@MnO_2	1.6	1MNa_2SO_4	79.3%retention after 5000 cycles	36
N-GNT@MoO_{3-x}//N-GNT@Na_xMnO_2	**2.2**	**1M Na_2SO_4**	**95.4% retention after 10000 cycles**	**In this work**
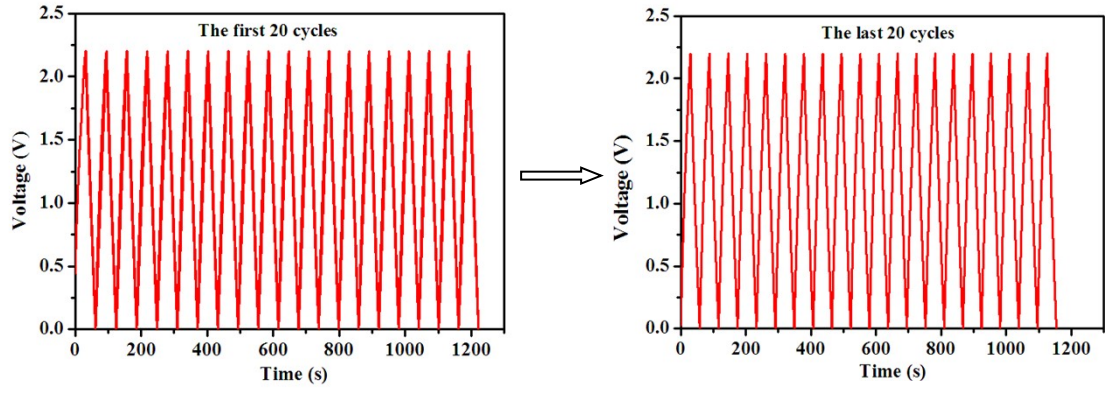
Fig. S9. GCD curves of the first and last 20 cycles for the assembled device during the continuous 10000 times charge/discharge process.

References

1 G.Y. Song, Z.J. Li, A.L. Meng, M. Zhang, K.H. Li, K.X. Zhu, *J. Alloys Compd.*, 2017, **706**, 147-155.

2 J. Zhao, Z.J. Li, T. Shen, X.C. Yuan, G.H. Qiu, Q.Y. Jiang, Y.S. Lin, G.Y. Song, A.L. Meng, Q.D. Li, *J. Mater. Chem. A*, 2019, **7**, 7918-7931.

3 J. Deng, J. G. Guo, X. L. Chen, *J. Am. Chem. Soc.*, 2020, **142**, 5234-5240.

4 J. P. Perdew, K. Burke, M. Ernzerhof, *Phys. Rev. Lett.*, 1996, **77**, 3865-3868.

5 K. Laasonen, A. Pasquarello, R. Car, C. Lee, D. Vanderbilt, *Phys. Rev. B*, 1993, **47**, 01042.

6 D. Vanderbilt, *Phys. Rev. B*, 1990, **41**, 7892-7895.

7 X. L. Wu, L. L. Jiang, C. L. Long, T. Wei, Z. J. Fan, *Adv. Funct. Mater.*, 2015, **25**, 1648.

8 Y. Q. Zhang, S. Yang, S. L. Wang, H. K. Liu, L. Li, S. X. Dou, X. Liu, *Small*, 2018, **14**, e1800480.

9 T. T. Gao, Z. Zhou, J. Y. Yu, D. X. Cao, G. L. Wang, B. Ding, Y. J. Li, *ACS Appl Mater Interf.*, 2018, **10**, 23834-23841.

10 W. Zong, F. L. Lai, G. J. He, J. R. Feng, W. Wang, R. Q. Lian, Y. E Miao, G. C. Wang, I. P. Parkin, T. X. Liu, *Small*, 2018, **14**, e1801562.

11 L. X. Feng, K. Wang, X. Zhang, X. Z. Sun, C. Li, X. Ge, Y. W. Ma, *Adv. Funct. Mater.*, 2018, **28**, 1704463.

12 R. Sahoo, D. T. Pham, T. H. Lee, T. H. T. Luu, J. Seok, Y. H. Lee, *ACS Nano*, 2018, **12**, 8494-8505.

13 M. Karuppannan, Y. Kim, Y. E. Sung, O. J. Kwon, *J. Mater. Chem. A*, 2018, **6**,

7522-7532.

14 N. M. Shinde, Q. X. Xia, J. M. Yun, P. V. Shinde, S. M. Shaikh, R. K. Sahoo, S. Mathur, R. S. Mane, K. H. Kim, *Electrochim. Acta*, 2019, **296**, 308-316.

15 J. G. Wang, H. Z. Liu, H. H. Sun, W. Hua, H. W. Wang, X. R. Liu, B. Q. Wei, *Carbon*, 2018, **127**, 85-92.

16 G. Y. Zhao, C. Chen, D. F. Yu, L. Sun, C. H. Yang, H. Zhang, Y. Sun, F. Besenbacher, M. Yu, *Nano Energy*, 2018, **47**, 547-555.

17 B. Wang, R. Hu, J. Zhang, *J. Am. Ceram. Soc.*, 2020, **103**, 1088-1096.

18 T. Wang, Q. J. Le, X. L. Guo, M. Huang, X. Y. Liu, F. Dong, J. T. Zhang, Y. X. Zhang, *ACS Sustain. Chem. Eng.*, 2018, **7**, 831-837.

19 T. Xiong, W. S. V. Lee, X. L. Huang, J. M. Xue, *J. Mater. Chem. A*, 2017, **5**, 12762-12768.

20 Q. J. Le, T. Wang, D. N. H. Tran, F. Dong, Y. X. Zhang, D. Losic, *J. Mater. Chem. A*, 2017, **5**, 10856-10865.

21 X. Q. Lang, H. Y. Mo, X. Y. Hu, H. W. Tian, *Dalton. Trans.*, 2017, **46**, 13720-13730.

22 R. B. Rakhi, B. Ahmed, D. Anjum, H. N. Alshareef, ACS Appl. Mater. Interf., 2016, **8**, 18806-18814.

23 W. Y. Ko, Y. C. Liu, J. Y. Lai, C. C. Chung, K. J. Lin, *ACS Sustain. Chem. Eng.*, 2018, **7**, 669-678.

24 Z. P. Ma, G. J. Shao, Y. Q. Fan, G. L. Wang, J. J. Song, D. J. Shen, *ACS Appl. Mater. Interf.*, 2016, **8**, 9050-9058.

25 Z. H. Huang, Y. Song, D. Y. Feng, Z. Sun, X. Sun, X. X. Liu, *ACS Nano*, 2018, **12**, 3557-3567.

26 B. S. Singu, K. R. Yoon, *Electrochim. Acta*, 2017, **231**, 749-758.

27 X. Y. Meng, L. Lu, C. W. Sun, *ACS Appl. Mater. Interf.*, 2018, **10**, 16474-16481.

28 X. Ma, L. Zhang, G. C. Xu, C. Y. Zhang, H. J. Song, Y. T. He, C. Zhang, D. Z. Jia, *Chem. Eng. J.*, 2017, **22**, 320.

29 W. D. He, Z. F. Liang, K. Y. Ji, Q. F. Sun, T. Y. Zhai, X. J. Xu, *Nano Res.*, 2018, **11**, 1415-1425.

30 O. Sadak, W. Z. Wang, J. H. Guan, A. K. Sundramoorthy, S. Gunasekaran, *ACS Appl. Nano Mater.*, 2019, **2**, 4386-4394.

31 Y. W. Sui, Y. M. Zhang, H. H. Hu, Q. Xu, F. Yang, Z. S. Li, *Adv. Mater. Interf.*, 2018, **5**, 1800018.

32 X. Zhao, W. Cai, Y. Yang, X. D. Song, Z. Neale, H. E. Wang, J. H. Sui, G. Z. Cao, *Nano Energy*, 2018, **47**, 224-234.

33 Y. D. Miao, X. P. Zhang, J. Zhan, Y. W. Sui, J. Q. Qi, F. X. Wei, Q. K. Meng, Y. Z. He, Y. J, Ren, Z. Z. Zhan, Z. Sun, *Adv. Mater. Interf.*, 2019, **2**, 1901618.

34 Z. J. Lv, Q. Zhong, Y. F. Bu, *Adv. Mater. Interf.*, 2018, **14**, 1800438.

35 N. M. Shinde, Q. X. Xia, J. M. Yun, R. S. Mane, K. H. Kim, *ACS Appl. Mater. Interf.*, 2018, **10**, 11037-11047.

36 Y. Li, J. Xu, T. Feng, Q. F. Yao, J. P. Xie, H. Xia, *Adv. Funct. Mater.*, 2017, **27**, 1606728.